ISSN 0015-4628, Fluid Dynamics, 2014, Vol. 49, No. 6, pp. 827–843. © Pleiades Publishing, Ltd., 2014.
Original Russian Text © A.V. Bazilevskii, A.N. Rozhkov, 2014, published in Izvestiya Rossiiskoi Akademii Nauk, Mekhanika Zhidkosti i Gaza, 2014, Vol. 49, No. 6, pp. 145–163.

Dynamics of Capillary Breakup of Elastic Jets

A. V. Bazilevskii and A. N. Rozhkov

Ishlinsky Institute for Problems in Mechanics, Russian Academy of Sciences,
pr. Vernadskogo 101, Moscow, 119526 Russia
e-mail: baz@ipmnet.ru, rozhkov@ipmnet.ru

Received March 27, 2014

Abstract—The tensile stress of threads appearing in the capillary breakup of jets of high-molecular polymeric solutions with concentrations of 0.003–0.03% is measured. As a stress sensor, the droplets adjacent to the thread were used. The forces acting on the threads are found. It is shown that, under the stretching, the rheologic behavior of the liquid in the thread differs from that in the conditions of contractile flow in the droplet. The inertial effects in the thinning of the threads between the jet droplets are analyzed.

Keywords: jet, droplet, breakup, polymeric solution, elasticity, relaxation time.

DOI: 10.1134/S0015462814060143

A capillary breakup of a jet is one of the fundamental processes of hydrodynamics. Despite of long history of its research, started from the works of Savart, Plateau, and Rayleigh [1–3], this process attracts the attention of researches until now. This is because the capillary jets are widely encountered in engineering. It is sufficient to mention ink jets [4], jet radiators of space stations [5], fuel atomization processes [6], coating technologies [7], and many other applications [8].

Of specific interest are polymeric jets, the forms of breakup of which differ from those for Newtonian fluids [4, 9–18]. Sometimes they become the elements of new technologies. For instance, due to polymeric additives the stability of jets increases, and the printing quality in ink jets is improved [4]. The effect of the formation of self-thinning threads in the breakup of jets or liquid bridges is used not only for the production of nanothreads [19, 20] but also as a method of studying the rheology of liquids under stretching [12, 21, 22].

The main feature of the breakup of polymeric jets is the transformation of bridges between the jet droplets into homogeneous liquid threads, slowly thinning with time (Fig. 1). A self-thinning thread between the jet droplets is the result of the capacity of polymeric liquids to accumulate considerable reversible deformations under stretching.

A theoretical analysis of the thread thinning process is based on specific assumptions on the liquid rheology, the flow character, and the stress distribution in the thread. In the first approximation, it is assumed [12] that the flow in the thread is inertialess, the thread is homogeneous in the length, and is axially symmetric. The existence of the thread is attributable to the balance between the external stresses (axial stress σ_x at the edges and the capillary pressure α/r) and the inner stresses (the tensor of extra stresses τ and the pressure p)

$$\sigma_x = \tau_x - p, \qquad -\alpha/r = \sigma_y = \tau_y - p.$$

Here, r is the thread radius, α is the surface tension coefficient, and the tensors $\boldsymbol{\sigma}$ and $\boldsymbol{\tau}$ are represented by the physical components in the cylindrical coordinates (x, y, φ) (Fig. 1c). Due to the orientation of polymeric molecules along the thread axis, $\tau_y = 0$ [23].

The further step in the formulation is the specification of the theological equation for the tensor $\boldsymbol{\tau}$ and the assumption that the axial physical component σ_x is much smaller than the radial physical component σ_y:

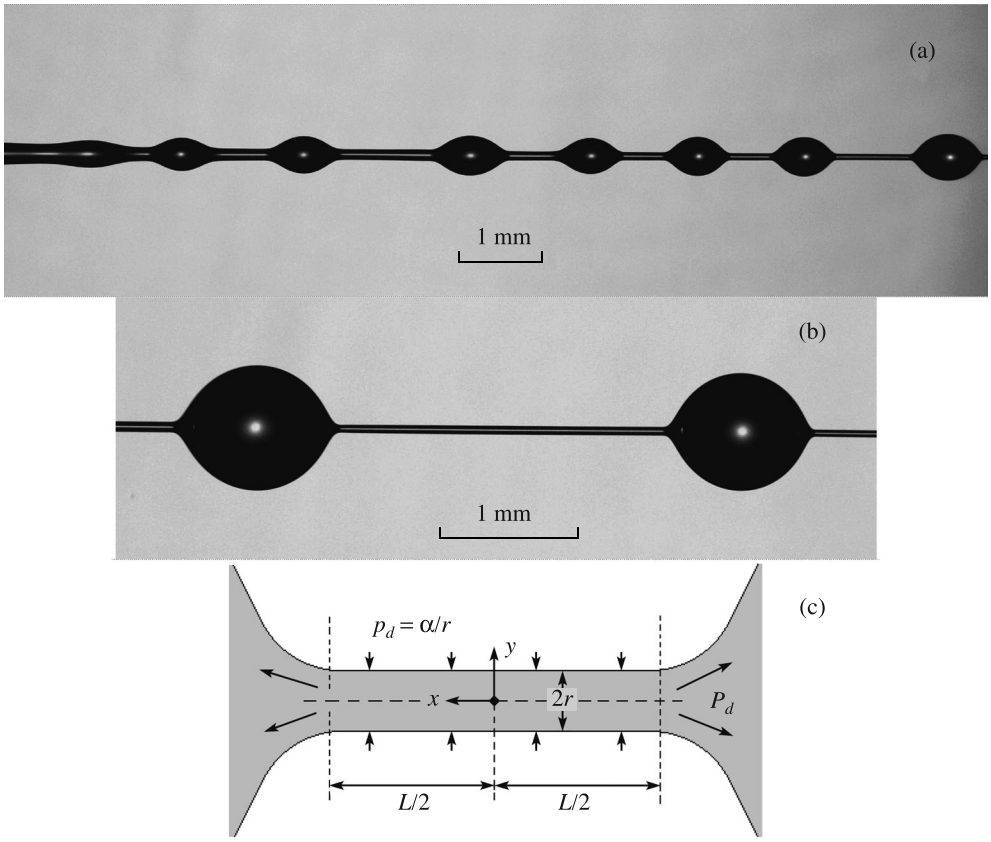

Fig. 1. Breakup of a jet of 0.01% PEO solution. The jets moves from left to right with a velocity of 1.7 m/s (a). Uniform cylindrical thread between the droplets in the breakup of a jet of 0.03% PEO solution (b). Model of the thread (c).

$|\sigma_x| \ll |\sigma_y = -\alpha/r|$ [12, 23, 24]. Along with the approximation $\sigma_x = 0$, other hypotheses also exist. Thus, in [25] it is assumed that $\sigma_x = \alpha/r$.

In the present study, we verify the assumption that the value of σ_x is finite and is determined by the process of liquid flow from the thread to the droplet and the capillary pressure in the droplet P_d. If the droplet is free of internal stresses in the motion in the droplet, then $\sigma_x = P_d$. However, if when the elastic liquid enters in the droplet the stresses relax with respect to the length, the appearance of a positive axial stress $\sigma_{\sim}\alpha/r$ is possible, which prompts the flow [26]. On the other hand, if the liquid is viscous, rather than elastic, the fluid deformation in the course of entering in the droplet creates the viscous stresses, which oppose the flow, $\sigma_x < 0$ [23, 25, 27].

Investigations of the breakup of polymeric jets are usually consist in recording the breakup patterns and comparing them with the analytical solutions or numerical results [28]. The information on the stress state of the liquid in the droplet plays the key role in understanding the jet breakup mechanisms of real liquids and the construction of the corresponding mathematical models. In addition, the knowledge of the stress distribution in the jet is necessary for the development of new rheometric tests of various liquids, carried out using jet breakup [29, 30].

This study was performed with the aim to develop a method of measurement and determination of the stresses in a fragmented jet of a real liquid. The stress state of the jet is, first of all, the tensile force F_f of the capillary thread connecting the neighboring droplets. Its value $F_f = 2\pi r\alpha + \sigma_x\pi r^2$ is determined as the sum of the force exerted on the surface $(2\pi r\alpha)$ and the forces acting in the volume $\pi r^2\sigma_x$.

At first sight, the problem of measurement of a variable force of the order of several tens of micronewtons in a moving jet seems to be very difficult. The first results of such experiments are given in [17]. The experiment involves a mechanical action on the jet. The jet flows out of a transversally oscillating nozzle,

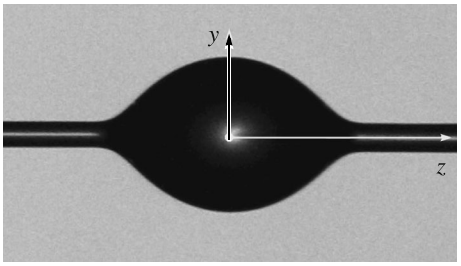

Fig. 2. Droplet of the jet with adjacent threads.

which results in the formation of an unusual, zigzag shape of the jet in the late stage of the jet breakup. In this jet, a pair of threads, adjacent to each droplet, forces the droplet to move along a curvilinear trajectory, the subsequent computer analysis of which makes it possible to determine the tensile forces on the threads.

In this study, we present an alternative method of measuring the tensile force on the thread directly in the polymeric jet, without any external action on the jet. The results of first experiments are published in [31].

1. THE METHOD

The measurement of the tensile force on the thread is based on the analysis of the shape of the droplet, adjacent to the thread. The axial forces exerted on the droplet by the threads cause a droplet deformation and a deviation of its shape from spherical. With increase in the tensile strength in the threads, this deviation increases. Thus, the droplet itself plays a role of a sensor of the force acting on the droplet from the thread.

Consider a jet droplet with adjacent threads in the cylindrical coordinates, with the z-axis directed along the thread axis (Fig. 2). Let the position $z = 0$ correspond to the maximal radius of the droplet $y = R_0$. It is assumed that both droplets, adjacent to the thread, are identical. The surface tension of the liquid is assumed to be constant and equal to its static value. We neglect the liquid motion inside the droplet and the corresponding inertia forces. The effect of internal stresses is assumed to be small. Thus, we consider a static droplet which is in the equilibrium under the action of only the capillary forces and the external stretching force F directed along the symmetry axis. Under these assumptions, the capillary pressure P_d and the stretching stress in the droplet are constant, and the droplet shape $R(z)$ satisfies the Laplace equation:

$$P_d = \alpha\left(\frac{1}{R}(1 + R'^2)^{-1/2} - R''(1 + R'^2)^{-3/2}\right) = \text{const}. \tag{1.1}$$

Here, α and ρ are the surface tension coefficient and the density of the liquid, $R' = dR/dz$, $R'' = d^2R/dz^2$.

The differential equation of the droplet shape (1.1) can be represented in dimensionless form

$$\frac{dY}{dZ} = Y_1, \qquad \frac{dY_1}{dZ} = \frac{1 + Y_1^2}{Y} - K(1 + Y_1^2)^{3/2}. \tag{1.2}$$

where $Y = R/R_0$ and $Z = z/R_0$ are the dimensionless radial and axial coordinates of the droplet profile, $K = P_dR_0/\alpha$, R_0 is the droplet radius in the section $z = 0$. The boundary conditions for Eqs. (1.2) take the form: $Y(0) = 1, Y_1(0) = 0$.

The parameter K characterizes the deviation of the droplet shape from spherical. For instance, $K = 2$ for a spherical droplet; $K = 1$ for a cylindrical droplet; and for intermediate variants $K \in (1, 2)$. This parameter also determines the stretching force:

$$F = 2\pi\alpha R_0 - P_d\pi R_0^2 = 2\pi\alpha R_0(1 - K/2).$$

In particular, $F = 0$ for a spherical droplet ($K = 2$) and $F = 2\pi\alpha R_0$ for a cylindrical droplet ($K = 1$).

The algorithm of the determination of F is as follows. By varying the parameter K and solving numerically Eq. (1.2), we can find such value of K for which the theoretical profile of the droplet $Y(Z, K)$ is most

close to the experimental tabular profile $Y_i(Z_i)$, $i = 1, \ldots, N$. The best approximation is determined using the least-square method, i.e. by the minimum of the expression [32]

$$\Phi(K) = (1/N)\sum_{1}^{N}\left[Y(Z_i,\ K)\ -\ Y_i(Z_i)\right]^2.$$

The value of K_* for which the functional $\Phi(K)$ attains the minimum was taken as the parameter to be found. Then, using the formula given above we calculated the stretching force $F = 2\pi\alpha R_0(1\ -\ K_*/2)$.

The use of the droplet as a force sensor has certain restrictions. First, the time of external action on the droplet should be much greater than the period of proper oscillations of the droplet. The period of the first mode of inertial oscillations of the spherical droplet is $T_i \approx (\rho R_0^3/8\alpha)^{1/2}$ [33]. Assuming for the estimate that $\rho = 1000$ kG/m^3, $\alpha = 0.07$ N/m, and $R_0 = 0.25$ mm, we obtain $T_i = 1/64 \times 10^{-4}$ s. Accordingly, the method is applicable for processes whose characteristic time is much greater than $T_i = 1/64 \times 10^{-4}$ s.

The liquid viscosity has a double effect. On one hand, it damps the proper oscillations of the droplet, which is a positive factor for using the method. On the other hand, it retards the droplet response on the variation of the acting force. This retardation can be estimated as $\Delta t_\nu \sim \eta R_0/\alpha$, η is the liquid viscosity [29]. For example, for $\eta = 0.01$ Pa×s, $\alpha = 0.07$ N/m, and $R_0 = 0.25$ mm the estimate gives the value $\Delta t_\nu = 3.6 \times 10^{-5}$ s. Hence, a small shear viscosity almost does not retard the response of the droplet shape on the force exerted.

Obviously, it is not possible to neglect the internal stresses in the liquid in the transition region between the thread and the droplet, where the elastic stresses in the flowing liquid are relaxed, but can still be large. This is why the solution of differential Eq. (1.2) can be used for the approximation of the droplet shape only outside this transition region.

2. THE EXPERIMENT

We investigated the aqueous solutions of polyethylene oxide (PEO, mean molecule mass $M = 4$ mln) and polyacrylamide (PAA, $M = 11$ mln) with the weight concentrations of 0.003, 0.01, and 0.03%. The static surface tension coefficient of the liquids under study was found using the hanging-droplet method [34]. The results are presented in Table 1. The static surface tension of the solutions PAA and PEO differs only slightly from that of water (see Table 1) and hence the effects of dynamic surface tension were not taken into account.

For the characteristic strain rates (100–1000 s^{-1}, the shear viscosity of the solutions PEO and PAA does not exceed 3 and 10 mPa s, respectively [35]. All measurements were performed at the temperature of 25–26°C.

The scheme of the experiment is shown in Fig. 3. For the creation of the jets, we used medical needles with inner diameters $d_i = 0.25$ and 0.34 mm. The needles were cut to the length of 10 mm, and their ends

Table 1

Liquid	Concentration, %	α, mN/m
Water	0	71.8 ± 0.3
PEO	0.003	67.3 ± 0.4
PEO	0.01	62.2 ± 0.3
PEO	0.03	62.1 ± 0.2
PAA	0.003	71.8 ± 0.2
PAA	0.01	72.1 ± 0.1
PAA	0.03	71.8 ± 0.2

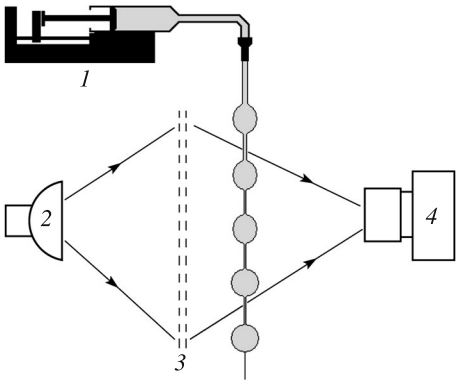

Fig. 3. Scheme of the experiment: (*1*) syringe pump, (*2*) pulse lamp, (*3*) condenser (Frenel lens), (*4*) photo camera.

were polished. The liquid was supplied by a KDS-200 syringe pump, connected with the outlet capillary (needle) by a flexible silicon pipe. The liquid flow rate was $Q = 5$ and 10 ml/min for needles with diameters $d_i = 0.25$ and 0.34 mm. The mean flow velocity $v_0 = 4Q/\pi d_i^2$ was equal to 1.69 and 1.84 m/s. The Reynolds number, estimated using the minimal shear viscosity of the solutions, was $\mathrm{Re} \sim 100$. The well-known estimate [36] of the length of formation of the Poiseuille velocity profile $l = 0.035\mathrm{Re} \times d_i$ indicates that the Poiseuille profile is formed inside the capillary ($l \sim 1$ mm). After reaching the nozzle, the profile relaxes to a plane form on the same length l. Hence, in the free jet, the velocity profile can be regarded as a plane one. The processing of the jet photographs showed that the diameter of the unperturbed part of the jet near the nozzle differs from the nozzle diameter by not more than 5%. Accordingly, in the calculations the initial velocity in the jet near the nozzle was taken equal to v_0.

The breakup of the jet was recorded using a Canon7D digital camera, supplied with a micro-objective and extension rings to enlarge the image scale. The resolution was 455 pixel/mm. A pulsing illumination (with the duration of 5 μs) in a passing light was used. The outlet capillaries were mounted on a vertical runner. This made it possible to displace the observation point to distances up to 100 mm along the vertical and record different stages of the jet breakup.

3. THE METHODS OF PROCESSING THE RESULTS

The analysis of the droplet shape and the calculation of the thread tensile stress were performed using a computer program of image processing, designed by the authors on the basis of the MatLab package.

The algorithm included the distinguishing of the jet edges and the measurement of the droplet profile with adjacent threads in the tabular dependence $R_i(z_i)$ $(i = 1, N_1)$, where the longitudinal coordinate z_i was initially determined accurate to a constant; $N_1 \sim 300$ is the number of measurement points. The interval $\Delta = z_{i+1} - z_i$ between the points corresponds to the pixel size in the photograph.

In measuring the thread profile, we used the technique of subpixel resolution, which consists in a linear interpolation of the intensity between the pixels. The value of a local threshold of intensity in determining the thread edge was chosen by photographing and processing a cylindrical calibre of a known diameter.

To establish the fitness of the maximum of the droplet radius to coordinate origin $z = 0$, we used a local polynomial approximation of the experimental dependence $R_i(z_i)$. A point z_* was found, at which the approximating function attained a maximum. The value R at this point was taken equal to the radius R_0. Using the transform $z_i = z_i - z_*$ $(i = 1, N_1)$, the location of the maximal radius was fitted to $z = 0$.

As mentioned above, the liquid flow in the droplet may result in a deviation of the droplet shape from static. This deviation is most clear in the transition region between the thread and the droplet. To track the effect of the droplet transition region on the results of measurement of the tensile stress on the thread and to eliminate this effect, we used the following scheme of processing the droplet shape.

For each droplet, the functional Φ was minimized with respect to the parameter K on a sequence of

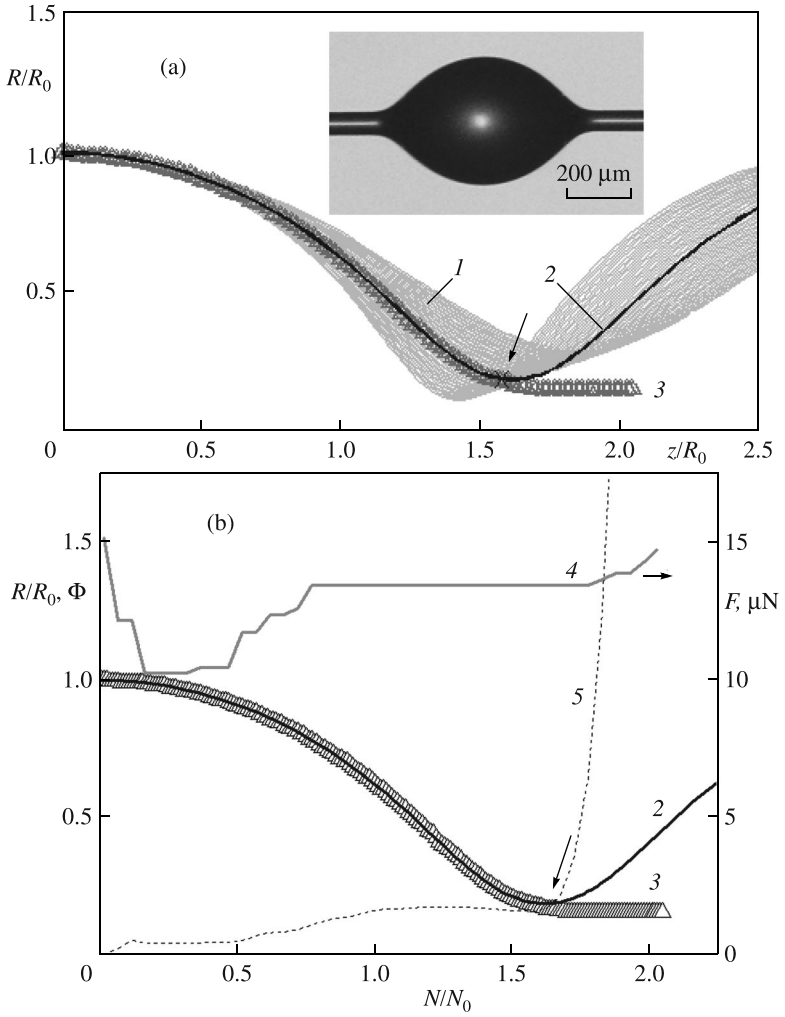

Fig. 4. Example of processing the image of 0.01% PEO droplet (a). Search for the best theoretical approximation: (*1*) theoretical profiles of the droplet for different values of K; (*2*) best variant ($K = 1.685$) for the measured profile of the droplet (*3*); the arrow shows the last experimental point analyzed. (b) Dependence of the stretching force F (*4*) and the functional Φ (*5*) along the droplet length; (*2*, *3*) theoretical and experimental profiles shown in (a); N_0 is the number of pixels falling within R_0; the arrow shows the limit, over which the effects of internal forces in the liquid should be taken into account.

expanding intervals of z. At each step, the $N-$th interval started from the coordinate $z = 0$ and ended by the coordinate z_N of the point N $(N < N_1)$ lying on the profile under consideration. Thus, the dependences of the parameters $K(N)$, $\Phi(N)$, and $\Phi(N)$ on the number of the points considered N were obtained. A typical example of the processing is shown in Fig. 4.

The reliability of the results increases with increase in the number of points N [32] under the condition that the use of the static model (1.2) does not goes beyond the range of its applicability. Indeed, starting from a certain fairly large number N, the quantities Φ and F are stabilized. At a certain critical value of N, a sharp growth of the value of Φ is observed, which is attributable to the fact that an interval of the jet with internal stresses in the liquid is included in the analysis. On this interval, the static model is no longer applicable, the theoretical description differs from the real profile of the jet, and Φ grows sharply. In Figs. 4a, 4b, the boundary of the range of applicability of model (1.2) is shown by arrows.

The measured value of the force was taken equal to the plateau in the graph $F(N)$.

To estimate the accuracy of measurement of the stretching force, we processed the spherical droplets without adjacent threads, when it is known a priori that $F = 0$. In this case, the numerical algorithm gave the values of the force of 0.1–0.2 μN, which corresponded to the error of an individual measurement. At the

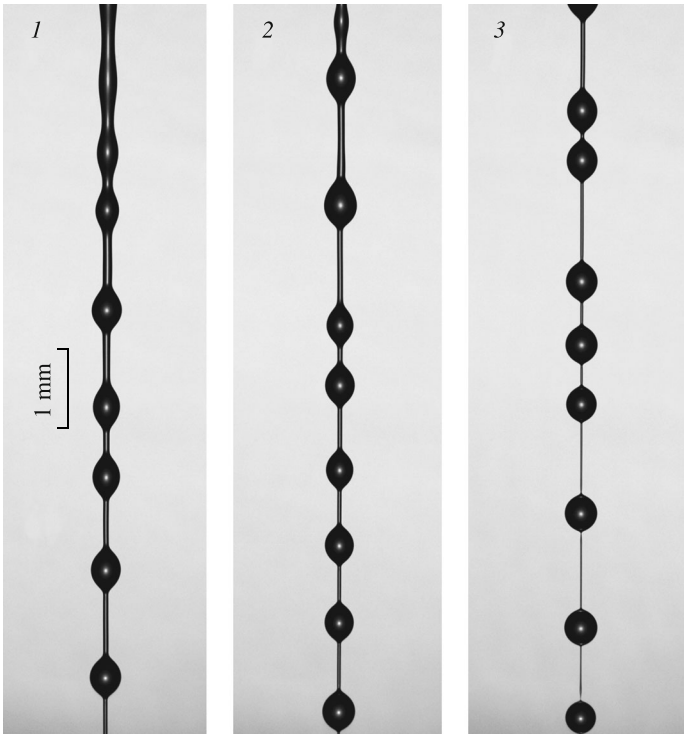

Fig. 5. Photographs of successive vertical segments of the jet (*1–3*) of 0.01% PEO solution. Initial velocity of the jet is 1.7 m/s.

same time, the range of measured tensile stresses on the threads was 5–45 μN. Accordingly, the accuracy of measurement of the stretching force using the method considered is sufficiently high ($\sim 1\%$).

The accuracy of measurement of the thread diameter is $\sim 1\%$ for thick threads and $\sim 5\%$ for the thinnest threads (diameter of 25 μm). To increase the accuracy of determination of the geometrical parameters of the jet, the image processing method used was calibrated by photographing two cylinders with diameters of 1.272 and 0.132 mm, measured by a high-accuracy micrometer.

Both threads adjacent to the same droplet were processed, i.e. the profiles were analyzed for $z > 0$ and $z < 0$. No noticeable difference for upper and lower threads was observed. This indicates the absence of the gravity force effect on the droplet shape in the vertical jet.

4. THE RESULTS AND ANALYSIS

In Fig. 5 we present the examples of photographs of PEO jet breakup at different distances from the nozzle outlet. Although no disturbances were applied to regularize the breakup, the latter has a regular nature (Fig. 1a).

The Rate of Jet Breakup

At first, we determined the time dependences of the thread diameter $2r(t)$. The thread diameter was measured in the middle between the droplets. The time t of motion of the thread element from the nozzle to the current location h was determined from the solution of the equation of constant-acceleration motion $h = v_0 t + gt^2/2$ for t, where $g = 9.8$ m/s^2 is the gravity force acceleration. The data for 0.01% solutions of PEO and PAA are shown in Fig. 6.

The thinning of an viscoelastic thread, whose rheology is described by the Oldroyd model, is given by the function [23]:

$$r = r_0 \exp(-t/3\theta). \tag{4.1}$$

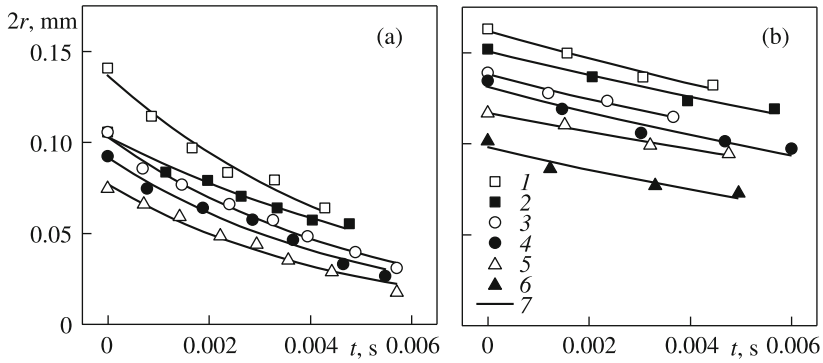

Fig. 6. Time dependences of the thread diameter, obtained as a result of processing the photographs of jet breakup (*1–6*) and the approximation by the exponential function $r = r_0 \exp(-t/3\theta)$ (*7*): (a) 0.01% PEO solution, (b) 0.01% PAA solution. Values of t are given accurate to a constant.

Table 2

Polymer	Concentration, %	θ, ms
PEO	0.003	0.68 ± 0.06
PEO	0.01	1.80 ± 0.14
PEO	0.03	4.88 ± 0.20
PAA	0.003	1.56 ± 0.17
PAA	0.01	6.44 ± 0.35
PAA	0.03	16.8 ± 3.70

where r_0 is the initial radius of the thread and θ is the relaxation time. The values of the relaxation times θ of the liquids considered are found by the approximation of the experimental data by theoretical dependence (4.1) (see Fig. 6 and Table 2).

Nonuniformity of the Thread Diameter

In the fragmented jet, the threads between the droplets seem to be uniform in the length (see Fig. 5). An enlarged fragment of the jet of a more concentrated solution is shown in Fig. 1b. However, the digital processing of the images indicates that characteristic contractions may appear on the thread near the droplet (Fig. 7). The diameter nonuniformity is the result of the fluid inertia. For a quantitative estimate of the action of inertia, we will use a system of quasi-one-dimensional motion equations of a thin capillary jet [15], without specification of the rheological equation for the liquid.

Integrating the momentum equations over the thread radius (Fig. 1c) and comparing the inertia term with the other terms of the sum, we obtain the condition when the inertia effect may be neglected:

$$\rho \int_x^{L/2} \left(\frac{\partial v}{\partial t} + v \frac{\partial v}{\partial x} \right) dx \ll \frac{2\alpha}{r}. \tag{4.2}$$

Here, x is the longitudinal coordinate measured from the middle of the thread, L is the thread length, and v is the axial velocity (Fig. 1c).

We will estimate the value of the integral on the left-hand side of Eq. (4.2), using the quantities $r(t)$ and L, measured in the experiment. For the uniaxial stretching, from the continuity equation we have

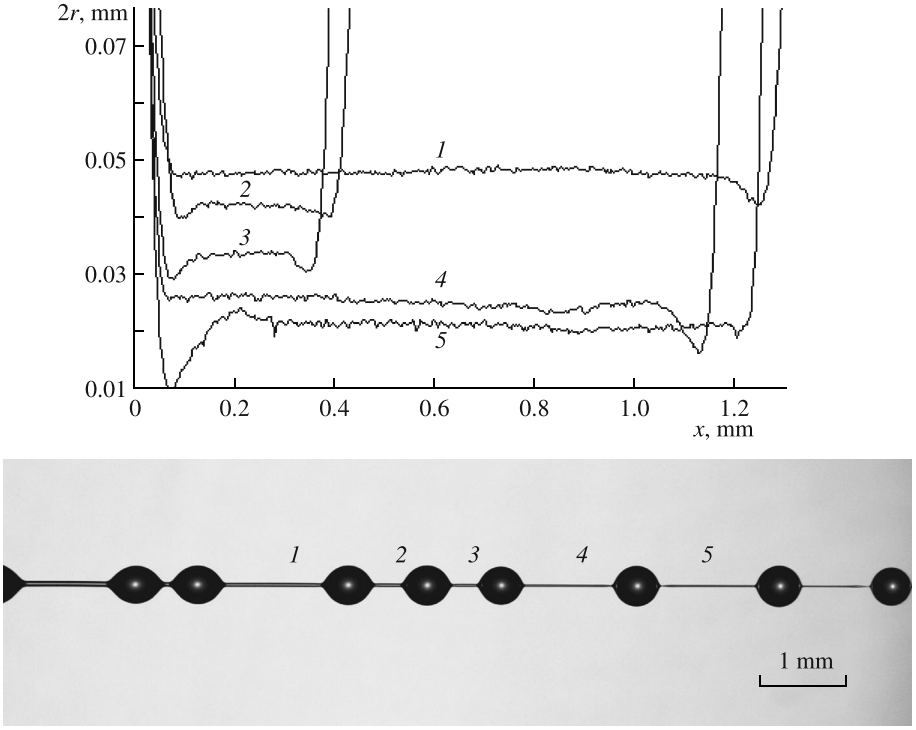

Fig. 7. Successive thread profiles (*1–5*) in the fragmented jet of 0.01% PEO solution. Coordinate x is determined accurate to a constant.

$v = (\partial v/\partial x)/x$ and $\partial v/\partial x = -2d(\ln r)/dt$, accordingly:

$$\frac{\partial v}{\partial t} + v\frac{\partial v}{\partial x} = \frac{\partial^2 v}{\partial x \partial t}x + 2\left(\frac{\partial v}{\partial x}\right)^2 x = -2\frac{d^2 \ln r}{dt^2}x + 8\left(\frac{d\ln r}{dt}\right)^2 x.$$

Substituting this result in Eq. (4.2), after the integration we obtain:

$$\rho\left(\frac{L^2}{4} - x^2\right)\left[4\left(\frac{d\ln r}{dt}\right)^2 - \frac{d^2 \ln r}{dt^2}\right] \ll \frac{2\alpha}{r}. \tag{4.3}$$

From (4.3) it follows that the effect of inertia forces is most pronounced in the middle of the thread ($x = 0$), and hence there the thread may be thinned slower than at the edges, becoming nonuniform in the length. The physical explanation of this fact is simple. In the middle of the thread, the capillary pressure accelerates a thread segment with the length $L/2$, while at the edge of the thread the length and the mass of the accelerated part is smaller, and the thread here is thinned faster. Thus, the condition of neglect of the fluid inertia in the thread thinning takes the form:

$$\frac{\rho L^2}{4}\left[4\left(\frac{d\ln r}{dt}\right)^2 - \frac{d^2 \ln r}{dt^2}\right] \ll \frac{2\alpha}{r}. \tag{4.4}$$

If, from an experiment or a theory, we know the thread thinning kinematics $r(t)$ then we can estimate the validity of the above inequality. For a thread thinning in accordance with the exponential law (4.1), from (4.4) it follows:

$$\rho v_i^2 \ll 2\alpha/r. \tag{4.5}$$

where $v_i = v(L/2) = L/3\theta$ is the velocity of the liquid supply in the droplet. Inequality (4.5) reflects the smallness of the pressure head at the edge of the thread ρv_i^2, as compared with the doubled capillary pressure in the thread α/r.

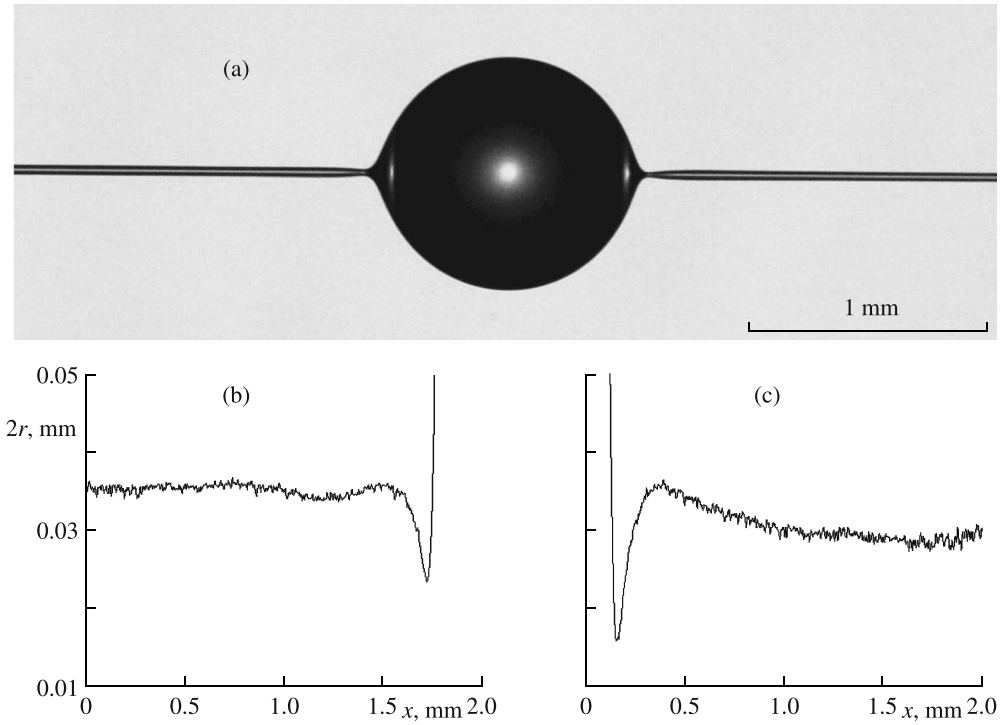

Fig. 8. Axisymmetric disturbances of the thread diameter to the left and to the right from the droplet (a) and their measured profiles (b, c). 0.03% PEO solution. Coordinate x is determined accurate to a constant.

Thus, from the condition of inertialess flow the uniformity of the thread in the length follows, since each thread element is thinned independently of the neighboring elements. It is assumed that the opposite statement is also valid, i.e. the uniformity in the length indicates the inertialess nature of thread thinning.

The substitution of the data $L = 1$ mm, $\alpha = 62$ mN/m, $\theta = 18$ ms, $r = 0.05$ mm, $\rho(L/3\theta)^2 = 34.3$ Pa, $2\alpha/r = 2480$ Pa for the threads of 0.01% solution of PEO in (4.5) shows that inequality (4.5) is valid. Nevertheless, the measured profiles of the threads in Fig. 7 show that, against the background of retainment of uniformity in the whole, a local nonuniformity of the thread starts to develop. This indicates a high 'sensitivity' of the longitudinal profile of the thread with respect to the inertia forces. Being manifested at the initial stage of thread thinning, the nonuniformity increases with the further thinning of the thread. The similar patterns of jet breakup were obtained in numerical simulations [37].

A local contraction at the thread edge retards the liquid motion along the thread, which results in the appearance of a droplet-shaped disturbance (Figs. 8–9). Earlier, such disturbances were not observed in the jet breakup. They were registered only in a single thread formed by thinning of a droplet of a concentrated polymeric solution between two discs [19, 20].

The appearance of the disturbances at the thread edge indicates the beginning of the thread breakup. The thread rupture process occurs fast, and it is difficult to catch it using individual photographs. Nevertheless, some photographs (Fig. 9) show that the rupture of the thread occurs at its ends.

Tension of the Thread

The processing of a large number of photographs of polymeric-jet breakup showed that the droplet shape is well described by the solution of Eq. (1.2), which is valid only for a static droplet. Certain deviations from the static profile are observed only in the transition region between the thread and the droplet (at distances of about 1–2 diameters of the thread). This indicates that the liquid motion in the droplet does not affect noticeably the droplet shape.

The results of measurement of the full stretching force F vs. the quantity $2\pi r\alpha$ are presented in Fig. 1. The graphs are obtained by the combination of the results of processing different droplets in instant photos

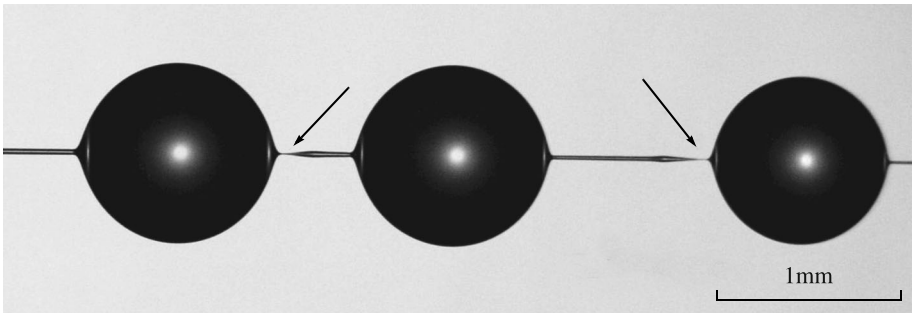

Fig. 9. Rapture (breakup) of the thread near the droplet. 0.03% PEO solution.

of the jet breakup. The diameter of the jet was taken equal to its value in the middle of the thread.

In Fig. 10, the measured value of F is compared with a hypothetical value equal to the difference $F_{f0} - F_i$, where F_{f0} is the tensile force of the thread, calculated with neglect of the liquid flow from the thread to the droplet, and F_i is a propulsion force, appearing due to the liquid flow into the droplet.

In the absence of the run-over effects, the axial stress in the thread σ_x is equal to the capillary pressure in the droplet P_d with the opposite sign $\sigma_x = -P_d$, and the tensile force is $F_{f0} = -P_d\pi r^2 + 2\pi r\alpha$. Using the formula $P_d = K\alpha/R_0$, we obtain $F_{f0} = (2\pi r\alpha)(1 - Kr/2R_0)$.

The propulsion force F_i is directed from the thread to the droplet and is equal to $F_i = \pi r^2\rho v_i^2$, where v_i is the inflow rate. For a thread with a length of L, thinning in accordance with the exponential law (4.1), the inflow rate is constant and equal to $v_i = Ld\ln r/dt = L/3\theta$. The mean length of the threads between the droplets of the jet is ~ 1 mm. With account of the values of θ given in Table 2, we can obtain the values of v_i and F_i for a thread with diameter of 0.1 mm (see Table 3). Clearly, the propulsion may noticeably affect the thinning of threads only for solutions with the concentration of 0.003%.

The dependence of the quantity $F_{f0} - F_i$ on $2\pi r\alpha$, obtained theoretically with account for the capillary pressure in the droplet and the propulsion force but with neglect of the possible flow of liquid from the thread to the droplet, is shown in Fig. 10 for four ranges of diameters of the droplets measured: $2R_0 \le 0.4$ mm, $0.4 < 2R_0 \le 0.6$ mm, $0.6 < 2R_0 \le 0.9$ mm, and $2R_0 > 0.9$ mm.

The data demonstrate a small but regular difference between the measurements and the theoretical predictions obtained using simple hypotheses. It is assumed that the difference is associated with the neglect of the process of liquid flow from the thread to the droplet.

Elastic Stresses in the Thread

The data in Fig. 10 make it possible to calculate the axial stress in the thread σ_x without the assumption of smallness of the end effects $\sigma_x = \Delta\sigma_x - P_d$, where $\Delta\sigma_x = (F - (F_{f0} - F_i))/\pi r^2$ is the contribution of the end effects in the axial stress. If $\Delta\sigma_x > 0$, the additional end stress pulls the liquid from the thread to the droplet, in the opposite case it prevents the flow into the droplet.

Table 3

Polymer	Concentration,%	v_i, m/s	F_i, μN ($2r = 0.1$ mm)
PEO	0.003	0.490	1.884
PEO	0.01	0.185	0.268
PEO	0.03	0.0683	0.0366
PAA	0.003	0.213	0.356
PAA	0.01	0.0517	0.0209
PAA	0.03	0.00198	0.000307

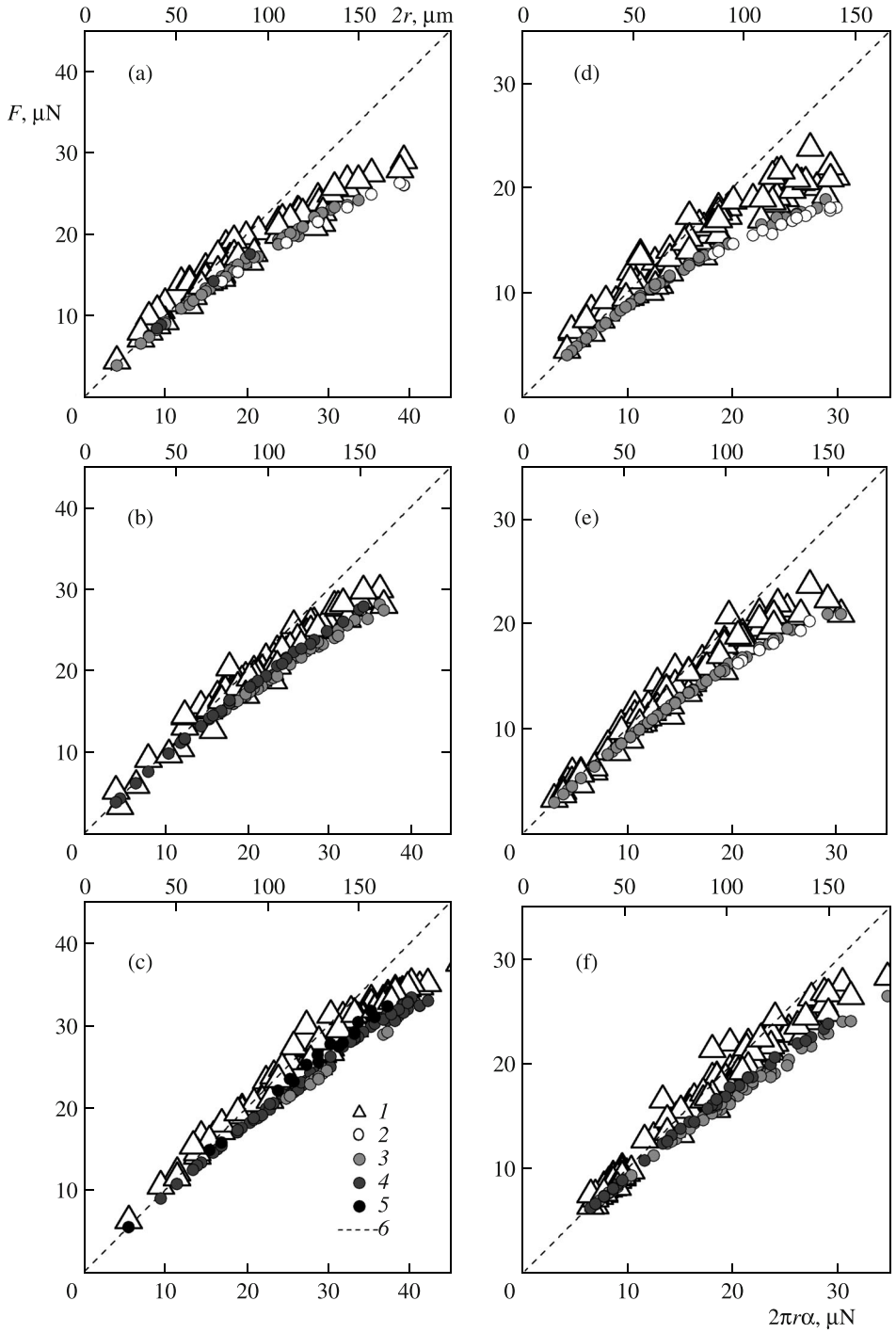

Fig. 10. Dependences of the measured stretching force F (*1*) and the theoretical value $(F_{f0} - F_i)$ (*2–5*) on $2\pi r\alpha$ for droplets of different diameters: (*2–5*) $2R_0 \le 0.4$ mm, $0.4 < 2R_0 \le 0.6$ mm, $0.6 < 2R_0 \le 0.9$ mm, $2R_0 > 0.9$ mm; (*6*) functional dependence $F = 2\pi r\alpha$; PAA $c = 0.003$, 0.01, 0.03% (a–c); PEO $c = 0.003$, 0.01, 0.03% (d–f).

Figure 11 shows the dependences of the quantities $\Delta\sigma_x/(\alpha/r)$ and $\Delta\sigma_x/\tau_x$ on the thread diameter, which indicate the level of the effect of liquid flow from the thread to the droplet, as compared to the capillary pressure $p_c = \alpha/r$ and the excess axial stress in the thread $\tau_x = \sigma_x + \alpha/r = \Delta\sigma_x P_d + \alpha/r$. The absence of the end effect means that $\Delta\sigma_x/(\alpha/r) = \Delta\sigma_x/\tau_x = 0$. When the end effect is maximal $\Delta\sigma_x/\tau_x = 0.5$ (see Sec. 5), $\Delta\sigma_x/(\alpha/r) = 1 - P_d/(\alpha/r)$. For thin threads, $(\alpha/r \gg P_d)\Delta\sigma_x/(\alpha/r) \cong 1$.

From Fig. 11, it follows that the end effect is small for liquids considered, and in the first approximation the value of this effect is independent of the thread diameter and the polymer concentration in the solution. Nevertheless, this effect takes place, and below we will discuss the reason for it. Note that the mean value $\Delta\sigma_x/\tau_x$ for liquids considered was equal to 0.196. Then, the balance between the internal and external stresses in the thread takes the form:

$$0.196\tau_x - P_d = \tau_x - \alpha/r.$$

Earlier, it was assumed that $-P_d = \tau_x - \alpha/r$ [12, 21, 23, 24]. We note that, with account of the mentioned balance of the forces in the thread, the exponential law of its thinning (4.1) retains. At the same time, the value of the elongation viscosity, determined from the experiment with a thinning thread, increases in 1.24 times.

Flow in the Droplet

In the inertialess approximation, when condition (4.5) is satisfied, the longitudinal component of the stress tensor σ_x is constant along the thread axis and is determined by the process of liquid flow from the thread to the adjacent microvolumes (droplets).

Following the approach of [16], we will consider the motion of the liquid near the droplet symmetry axis (Fig. 12), where the liquid is subjected to an unilateral compression, and the stresses in it relax. When the effects of the orientation viscosity are larger than those of the shear viscosity, a quasi-one-dimensional equation of motion written for the symmetry axis of the droplet takes the form [16]:

$$\rho\left(\frac{\partial v}{\partial t} + v\frac{\partial v}{\partial s}\right) = \frac{\partial}{\partial s}(\tau - p) - \frac{\tau}{v}\frac{\partial v}{\partial s}. \tag{4.6}$$

where s is the longitudinal coordinate, v is the velocity on the droplet axis, τ is the axial component of the tensor of excessive stresses inside the droplet. The values of v and τ are assumed to be constant across the flow section.

In the inertialess approximation, the integration of (4.6) from s_0 to ∞ gives the value of the full axial stress in the thread:

$$\sigma_x = (\tau\ p)_{s=s_0} = -P_d - \int_{s_0}^{\infty} \frac{\tau}{v}\frac{\partial v}{\partial s}\,ds. \tag{4.7}$$

To estimate the integral in (4.7), we assume the radial character of the flow on the droplet axis:

$$v = \frac{Q}{s^2}, \qquad \frac{\partial v}{\partial s} = -\frac{2Q}{s^3}, \qquad Q = \frac{q}{2\pi(1 - \cos\psi_0)}. \tag{4.8}$$

where $q = \pi r^2 v_i$ is the volume flow rate of the incoming liquid, v_i is the velocity at the end of the thread ($v_i = L/3\theta_0$ for the exponential thinning (4.1)), r is the thread radius, and ψ_0 is half-angle at the cone apex (Fig. 12).

To describe the thread thinning and the rheology of the flow in a microvolume, we will use the Oldroyd-B theological relation [23]:

$$\left(\frac{\partial \tau}{\partial t} + v\frac{\partial \tau}{\partial s}\right) = 2\tau\frac{\partial v}{\partial s} - \frac{\tau}{\theta_1}. \tag{4.9}$$

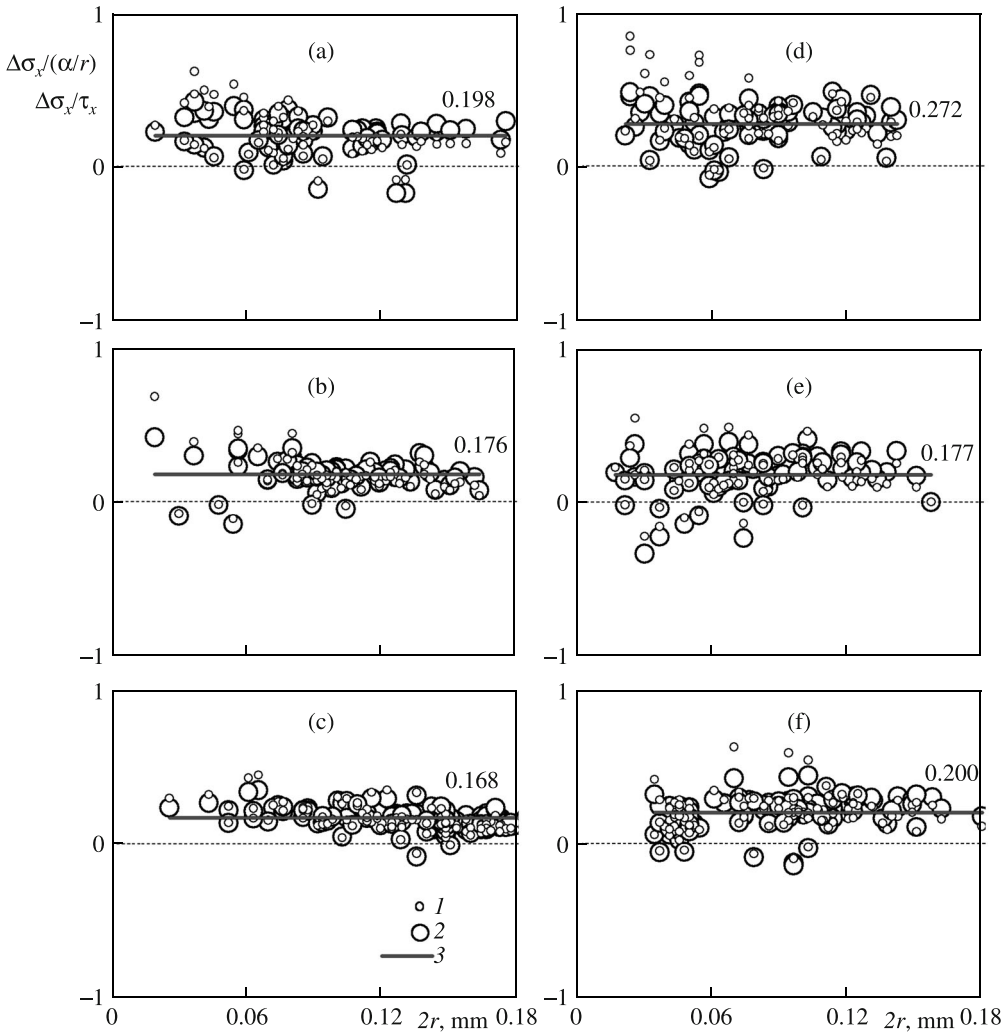

Fig. 11. Dependences $\Delta\sigma_x/(\alpha/r)$ (*1*) and $\Delta\sigma_x/\tau_x$ (*2*) on the thread diameter; PAA $c = 0.003$, 0.01, 0.03% (a–c); PEO $c =$ 0.003, 0.01, 0.03% (d–f); (*3*) approximation of the dependence $\Delta\sigma_x/\tau_x$ by a constant value; the value of the approximation parameters is shown in the graphs.

In this relation, the stress relaxation time θ_1 may differ from the relation time θ in the stretching of the thread.

We assume that the stresses start to relax at the point where the radius of the conical jet is equal to the thread radius: $s_0 = r/\sin\psi_0 \approx r/\psi_0$. The flow in the droplet is assumed to be quasi-steady. The steadiness condition is satisfied when the time of motion of a liquid particle in the droplet R_0/v_i is much smaller than the characteristic time of thread thinning $3\theta = L/v_i$, i.e. when the droplet radius is much smaller than the thread length: $R_0 \ll L$.

Substituting kinematic relations (4.8) in (4.9), we obtain the differential equation:

$$\frac{d\ln r}{ds} = -\frac{4}{s} - \frac{s^2}{\theta_1 Q}, \qquad \tau(s_0) = \tau_x.$$

After the integration with account of $Q \cong r^2 v_i/\psi_0^2$ for small ψ_0, we obtain the distribution of the stresses in the droplet:

$$\tau = \tau_x \xi^{-4} e^{A(1-\xi^3)}, \qquad \xi = \frac{s}{s_0}, \qquad A = \frac{r}{3v_i\theta_1\psi_0} = \frac{r}{\psi_0 L}\frac{\theta}{\theta_1}.$$

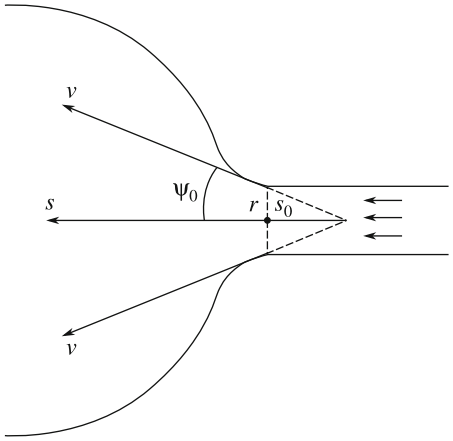

Fig. 12. Scheme of flow from the thread to the droplet.

Substituting this solution in (4.7) gives:

$$\sigma_x = -P_d + 2\tau_x \int_1^\infty \frac{e^{A(1-\xi^3)}}{\xi^5}\, d\xi. \tag{4.10}$$

Thus, the end effect is determined by the integral

$$\frac{\Delta\sigma_x}{\tau_x} = 2\int_1^\infty \frac{e^{A(1-\xi^3)}}{\xi^5}\, d\xi.$$

This effect is maximal in the case of elastic behavior of the liquid in the flow into the droplet $A = \psi_0^{-1}(\theta/\theta_1) \times (r/L) \to 0$ and attains $\Delta\sigma_x/\tau_x = 1/2$. The minimal effect, $\Delta\sigma_x/\tau_x = 0$, is observed for the instant relaxation of the stresses in the droplet:

$$A = \psi_0^{-1}(\theta/\theta_1) \times (r/L) \to \infty.$$

The character of the dependence of $\Delta\sigma_x/\tau_x$ on the diameter, shown in Fig. 13a is close to that, observed in the experiment (Fig. 11). The calculation results for different values of the parameter A are presented in Fig. 13b. The mean value of $\Delta\sigma_x/\tau_x$ obtained in the experiment is equal to 0.196, which corresponds to $A \approx 1.55$. In the experiment, the ratio of the thread radius to its length r/L varies on the range 0.01–0.1. We assume that $\psi_0 \approx 1$, i.e. almost the maximal possible angle (115 degrees) of the radial flow in the thread. Then, for the description of the experimental results, we should assume that $\theta/\theta_1 = 0.0155$–0.155, i.e. the stress relaxation time in the compressing flow in the droplet is in many times smaller than the relaxation time in the stretching of the thread. The fast relaxation of the stresses in the droplet is also indicated by the fact that the entire length (up to the region of transition into the thread) the droplet shape is well approximated by the solution of Eq. (1.2), describing the static droplet shape.

The statement that the stresses in the droplet relax instantaneously when the liquid enters in the droplet, and hence $\sigma_x = -P_d$ ($\ll p_c$) [12, 21, 23, 24], was formulated earlier only as a hypothesis. In the present study, we obtained the experimental data which confirm this approximation. The physical reasons for such behavior of the polymeric solution are still unclear, and their explanation lies beyond the scope of this paper.

The results obtained give a new insight on the rheological behavior of polymeric solutions in elongation flows. In particular, we note that the calculations of breakup of polymeric jets, known in the literature, which are usually based on a rheological model with a single relaxation time, independent of the type and rate of deformation, conceptually cannot describe the real jet breakup process. Moreover, we may assert that the calculation of any elongational flow, including the transition from the stretching deformation

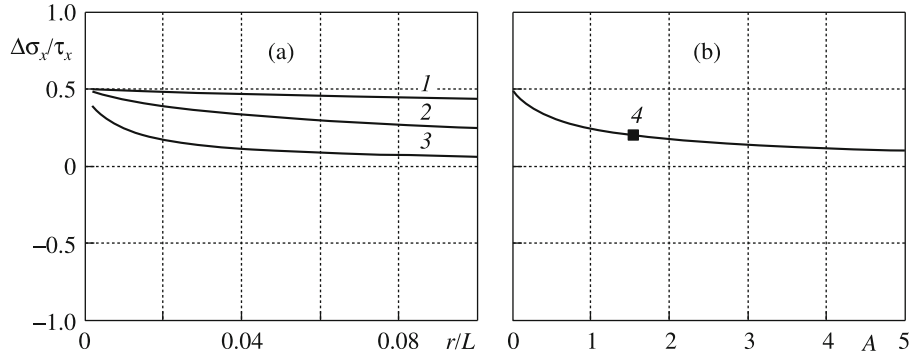

Fig. 13. End effect of liquid run-over as a function of the radius-to-length ratio of the thread (a) for $\psi_0 = 1$, $\theta/\theta_1 = 1$, 0.1, 0.01 (*1–3*) and the dimensionless parameter $A = (r/L) \times (\theta/\theta_1) \times (1/\psi_0)$ (b), (*4*) value $A = 1.55$ for $\Delta\sigma_x/\tau_x = 0.1963$.

to the compression deformation (for example, the liquid motion through a channel with a variable cross section) must take into account the change of the rheological behavior of the liquid with the change of the deformation type.

Summary. A method of measurement of the tensile force of threads between the droplets of a polymeric jet, based on the analysis of photographs of capillary breakup of polymeric jets, is developed.

The value of the stress in the thread is found, and the quantitative estimates of the end effect of liquid flow from the thread into the droplet are obtained. The effect is manifested in the elastic pulling up of the thread, which results in additional growth of the stresses. The value of the effect is small for the polymers considered, but may be significant for other polymeric liquids.

The analysis of the data obtained makes it possible to conclude that the rheological behavior of the liquid in the flows in the thread and in the adjacent droplet are different. This is manifested in a sharp decrease in the liquid relaxation time in the process of flow from the thread into the droplet, as compared to the liquid relaxation time in a thinning thread.

A high sensitivity of the forms of jet breakup with respect to the action of inertia forces is detected.

This work was supported by RFBR (No. 12-08-00067a).

REFERENCES

1. F. Savart, "Mémoire sur la Constitution des Veines Liquides Lancées par des Orifices Circulaires en Mince Paroi," Ann. Chim. (Paris) **53**, 337–386 (1833).
2. J. Plateau, *Statique Expérimentale et Théorique des Liquides Soumis aux Seules Forces Moleculaires. V. 1, 2* (Gauthier-Villars et Cie, Paris, 1873).
3. Rayleigh, "On the Instability of Jets," Proc. London Math. Soc. **10**, 4 (1879).
4. A.V. Bazilevskii, D.D. Meier, and A.N. Rozhkov, "Dynamics and Breakup of Pulse Microjets of Polymeric Liquids," Fluid Dynamics **40** (3), 376–392 (2005).
5. G.V. Konyukhov and A.A. Koroteev, "Study of Generation and Collection of Monodisperse Droplets Flows in Microgravity and Vacuum," Journal of Aerospace Engineering **20** (2), 124–127 (2007).
6. Yu.F. Dityatkin, L.A. Klyachko, V.V. Novikov, and V.I. Yagodkin, *Liquid Atomization* [in Russian] (Mashinostroenie, Moscow, 1977).
7. M.S. Owens M.S., M. Vinjamur, L.E. Scriven, and C.W. MacOsko, " Misting of Non-Newtonian Liquids in Forward Roll Coating," J. Non-Newtonian Fluid Mech. **166** (19–20), 1123–1128 (2011).
8. J. Eggers and E. Villermaux, "Physics of Liquid Jets," Reports on Progress in Physics **036601**, 1–79 (2008).
9. M. Goldin, J. Yerushalmi, R. Pfeffer, and R. Shinnar, "Breakup of a Laminar Capillary Jet of a Viscoelastic Fluid," J. Fluid Mech. **38**, 689–711 (1969).
10. M. Gordon, J. Yerushalmi, and R. Shinnar, "Instability of Jets of Non-Newtonian Fluids," Trans. Soc. Rheol. **17** (2), 303–324 (1973).
11. V.M. Entov, V.I. Kordonskii, V.A. Kuz'min, et al., "Investigation of Breakup of Jets of Rheologically Complex Liquids," Prikl. Mekh. Tekh. Fiz., (3), 90–98 (1980).

12. A.V. Bazilevskii, S.I. Voronkov, V.M. Entov, and A.N. Rozhkov, "Orientation Effects in the Breakup of Jets and Threads of Dilute Polymer Solutions," Dokl. Akad. Nauk USSR **257** (2), 336–339 (1981).
13. S.L. Goren and M. Gottlieb, "Surface-Tension-Driven Breakup of Viscoelastic Liquid Threads," J. Fluid Mech. **120**, 245–266 (1982).
14. V.M. Entov and A.L. Yarin, "Dynamics of Free Jets and Films of Viscous and Rheologically Complex Liquids," in: *Advances in Science and Technology. Ser. Mechanics of Fluids and Gases* [in Russian] (VINITI, Moscow, 1984), **18**, pp. 112–197.
15. A.L. Yarin, *Free Liquid Jets and Films: Hydrodynamics and Rheology* (Wiley, New York, 1993).
16. A.N. Rozhkov, "Dynamics and Breakup of Viscoelastic Liquids (A Review)," Fluid Dynamics **40** (6), 835–853 (2005).
17. A.V. Bazilevskii and A.N. Rozhkov, "Dynamics and Breakup of Zigzag-Like Jets of Polymeric Liquids," Fluid Dynamics **41** (4), 493–503 (2006).
18. C. Clasen, J. Bico J., V.M. Entov, and G.H. McKinley, "Gobbling Drops': the Jetting-Dripping Transition in Flows of Polymer Solutions," J. Fluid Mech. **636**, 5–40 (2009).
19. R. Sattler, C. Wagner, and J. Eggers, "Blistering Pattern and Formation of Nanofibers in Capillary Thinning of Polymer Solutions," Phys. Rev. Lett. **100**, 164502-1- 164502-4 (2008).
20. R. Sattler, S. Gier, J. Eggers, and C. Wagner, "The Final Stages of Capillary Break-up of Polymer Solutions," Phys. Fluids **24**, 023101-1-023101-21 (2012).
21. P. Schümmer and K.H. Tebel, "A New Elongational Rheometer for Polymer Solutions," J. Non-Newtonian Fluid Mech. **12**, 331–347 (1983).
22. S.L. Anna and G.H. McKinley, "Elasto-Capillary Thinning and Breakup of Model Elastic Liquids," J. Rheol. **45**, 115–138 (2001).
23. A.V. Bazilevskii, V.M. Entov, and A.N. Rozhkov, "Breakup of a Bridge of the Oldroyd Liquid—Method of Rheological Testing of Polymer Solutions," High-Molecalar Compounds, Ser. A 43 (7) 1161–1172. 24 (2001).
24. V.M. Entov and E.J. Hinch, "Effect of a Spectrum Relaxation Times on the Capillary Thinning of a Filament of Elastic Liquids," J. Non-Newtonian Fluid Mech. **72**, 31–53 (1997).
25. M. Stelter, G. Brenn, A.L. Yarin, et al., "Validation and Application of a Novel Elongational Device for Polymer Solutions," J. Rheol. **44** (3), 595–616 (2000).
26. A.N. Rozhkov, "Dynamics if Threads of Dilute Polymer Solutions," Inzh. Fiz. Zh. **45** (1), 72–80 (1983).
27. A.V. Bazilevskii, "Dynamics of Horizontal Viscoelastic-Fluid Filaments", Fluid Dynamics **48** (1), 111–124 (2013).
28. C. Clasen, J. Eggers, M.A. Fontelos, et al., "The Beads-on-String Structure of Viscoelastic Jets," J. Fluid Mech. **556**, 283–308 (2006).
29. A.N. Aleksandru, A.V. Bazilevskii, V.M. Entov, et al., "Breakup of a Capillary Bridge of Suspension," Fluid Dynamics **45** (6), 952–964 (2010).
30. A.V. Bazilevskii, V.M. Entov, and A.V. Rozhkov, "Breakup of a Liquid Bridge as a Method of Rheological Testing of Biological Liquids," Fluid Dynamics **46** (4), 613–622 (2011).
31. A. Bazilevsky, A. Rozhkov, and A. Stavitsky, "Stresses in the Filaments of Polymer Solutions," in: *Progr. and Trends Rheol. IV. Proc. 4th Eur. Rheology Conf. Sevilla. 1994, Sevilla, Spain* (Steinkopff, Darmstadt 1994), pp. 468–470.
32. P.V. Novitskii and I.A. Zograf, *Estimate of Measurement Data Errors* [in Russian] (Energoizdat, Leningrad, 1991).
33. Rayleigh (1896), *The Theory of Sound. Second edition, V. 2* (MacMillan, London. Reprinted by Dover, New York, 1945).
34. A. Adamson, *Physical Chemistry of Surfaces* (Wiley, New York, 1990).
35. A. Rozhkov, B. Prunet-Foch, and M. Vignes-Adler, "Dynamics and Disintegration of Drops of Polymeric Liquids," J. Non-Newtonian Fluid Mech. **134**, 44–55 (2006).
36. R.B. Bird, W.E. Stewart, and E.N. Lighfoot, *Transport Phenomena* New York, Wiley, 1960.
37. J. Li and M.A. Fontelos, "Drop Dynamics on the Beads-on-String Structure of Viscoelastic Jets: A Numerical Study," Phys. Fluids **15**, 922–936 (2003).